8.5 ELASTIC BACKSCATTER LIDAR OBSERVATIONS OF SEA-BREEZE FRONTS IN DIXON, CALIFORNIA

Shane D. Mayor*, Scott M. Spuler, Bruce M. Morley, Stephan C. Himmelsbach, Robert A. Rilling, Tammy M. Weckwerth, Edward G. Patton, and Donald H. Lenschow

National Center for Atmospheric Research, Boulder, Colorado

1. INTRODUCTION

Ground-based, scanning, elastic backscatter lidars offer exceptional ability to observe the structure and motion of land- and sea-breeze fronts. As an example, Mayor and Eloranta (2001) presented University of Wisconsin Volume Imaging Lidar (UW-VIL) observations of a land-breeze advecting offshore over Lake Michigan in the winter of 1997. Those observations revealed a very shallow offshore flow that terminated sharply approximately 2 km offshore. Algorithms applied to the data delineated the position of the front and velocity of the aerosol structures on both sides of the front. The observations were used to validate a numerical simulation of the event (de Boer, 2004; de Boer et al., 2004, 2005). Unfortunately, the ocular hazard associated with the UW-VIL prevents it from being widely deployed—especially near urban areas or busy coastlines.

Recognizing the value of such observations, the Earth Observing Laboratory (EOL) at the National Center for Atmospheric Research (NCAR) began developing an eye-safe version of the UW-VIL in 2002. In 2007, the NCAR Raman-shifted Eye-safe Aerosol Lidar (REAL) was deployed from mid-March to mid-June near Dixon, California, for the Canopy Horizontal Array Turbulence Study (CHATS). Figure 1 shows the instrument at this experiment. This was the second deployment for REAL in a National Science Foundation (NSF) sponsored field campaign. The goal of the deployment was to test REAL's ability to detect very fine-scale turbulent coherent structures, such as ejections and sweeps, over a forest canopy. A large walnut orchard served as an idealized forest canopy in which towers supporting arrays of closely spaced instruments were installed. The location of the site, approximately 100 km from the Pacific Ocean (see Fig. 2), provided an opportunity to observe several sea-breeze frontal passages.

* *corresponding author address:* Shane D. Mayor, National Center for Atmospheric Research, P. O. Box 3000, Boulder, CO 80307-3000; *email*: shane@ucar.edu

Figure 1: The NCAR REAL as deployed for the Canopy Horizontal Array Turbulence Study.

2. INSTRUMENT

The NCAR REAL is described in detail by Mayor and Spuler (2004) and Spuler and Mayor (2005). Although not yet in the NSF deployment pool, REAL is available for use by the university community by submitting a request to the NSF. The lidar is unique in that it operates at 1.5-microns wavelength. This wavelength falls within a narrow region of the near-infrared portion of the optical spectrum that offers maximum eye-safety. By operating at this wavelength, a lidar can transmit high pulse energy safely. REAL is eye-safe at 0 meters range for a 10 second unaided stare according to ANSI standards. An additional important feature for lidar operation in urban regions is an invisible beam. Other eye-safe lidars with invisible beams exist, but high-pulse energy operation at 1.5 microns enables use of an analog direct detection receiver and rapid scanning. Rapid scanning enables one to create time-lapse animations of flow as evidenced by variability in the aerosol backscatter. The system, as configured for CHATS, transmitted 10 laser pulses per second.

Just prior to the deployment to CHATS, REAL benefited from several substantial improvements. They include (1) the ability to run continuously and unattended for periods of several weeks, (2) the ability to interleave the collection RHI and PPI scans in order to provide horizontal and vertical animations during the same period, (3) backscatter polarization sensitivity (Mayor et al., 2007), and (4) remote control and near-real-time

Figure 2: The NCAR REAL was located approximately 100 km from the Pacific Ocean during the CHATS.

perusal of "Quick-look" scan images via the internet. Final data products are now delivered in NetCDF format and programs have been written in Matlab and IDL to make data access and custom data processing easier. Analog to digital signal processing rates were increased to 100 million samples per second for CHATS in order to record backscatter at 1.5-meter intervals. Detection signal amplifier electronics were rebuilt in an effort to increase receiver bandwidth and sense finer scale variability along the beam.

3. LOCATION

The NCAR REAL was installed among a wide variety of agricultural fields approximately 5 kilometers north of the city of Dixon, California (see Fig. 2). The site was chosen for its exceptional flatness and clear vantage of the northern edge of a very large walnut orchard located 1.4 km to the south. Arrays of in situ sensors were installed on towers in the orchard in order to investigate the interaction of boundary-layer scale fluid mechanics and the canopy-imposed influences on momentum and scalar exchange. Therefore, the main observation site in CHATS was a custom tower structure supporting horizontal arrays of closely spaced in situ sensors located in the orchard about 1.71 km from the lidar. It was 12 meters tall. Additionally, a 30 meter tall tower was located 1.61 km from the lidar site. Trees in the orchard were approximately 10 meters tall. This location allowed the lidar to routinely make PPI scans at elevation angles as low as 0.2 degrees above horizontal without interference from the orchard trees.

Figure 3: Looking south over the CHATS site as photographed by Carlye Calvin from the Duke University helicopter. The REAL is located at the bottom center of the picture.

4. OBSERVATIONS

The lidar was operated nearly continuously and mostly unattended at CHATS from 15 March to 11 June, 2007. Visits by staff every few weeks were made to change laser flashlamps and hard disks. Only a few interruptions lasting more than an hour, and sometimes as long as a few days, occurred due to electrical power disruptions and, in one case, failure of a commercial digitizer card. The result of the deployment is very large data set—containing over 2.5 TB of raw data from over 1850 hours of operation. The lidar is equipped with a precipitation sensor in order suspend operations during rain events.

A variety of scan strategies were conducted with the lidar during the experiment. Since the primary goal was to observe very fine-scale turbulent coherent structures over the orchard, the lidar was often programmed to make narrow RHI and PPI scans directly over the orchard. However, because ideal conditions for the in situ component of the experiment only occurred when the wind was from the south, we collected wide angle RHI and PPI scans at other times. In many cases, we collected RHI and PPI scans in a continuously alternating fashion so that time-lapse animations of both horizontal and vertical atmospheric structure could be obtained simultaneously.

For this paper, we have selected the three most dramatic sea-breeze cases. Other, less dramatic and more complex cases exist in the data set.

4.1 15 March

During this case, the lidar was recording data to 10.7 km range. Flow near the surface and ahead of the front as evidenced by aerosol motion in the lidar animations

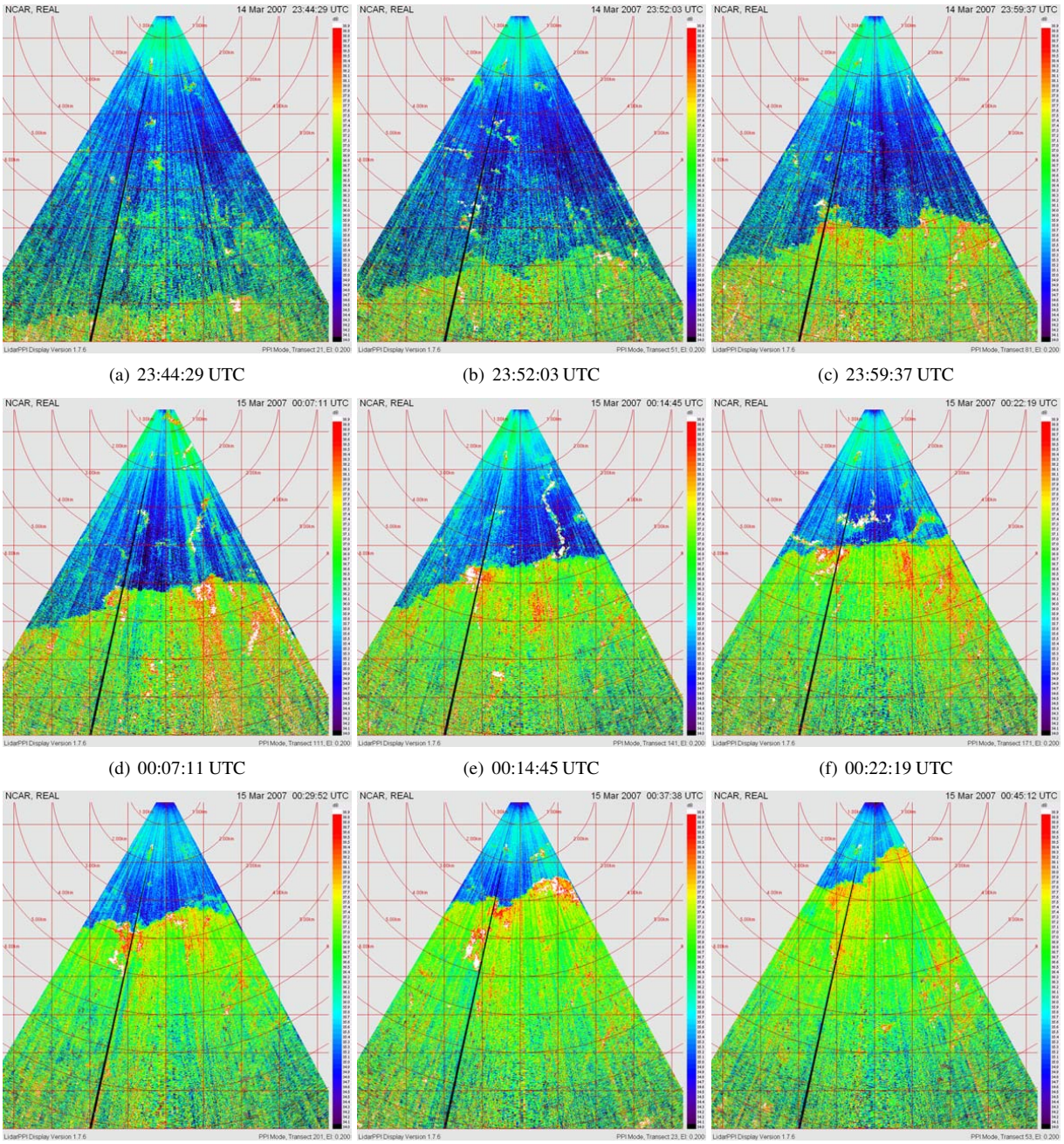

(a) 23:44:29 UTC (b) 23:52:03 UTC (c) 23:59:37 UTC

(d) 00:07:11 UTC (e) 00:14:45 UTC (f) 00:22:19 UTC

(g) 00:29:52 UTC (h) 00:37:38 UTC (i) 00:45:12 UTC

Figure 4: Near-horizontal PPI scans from 23:44:29 UTC on 14 March 2007 to 00:45:12 UTC on 15 March 2007. The elevation angle of the scans is 0.2-degrees above horizontal. Range rings and grid lines are drawn at 1 km intervals. The maximum range shown directly south of the lidar site is 9 km.

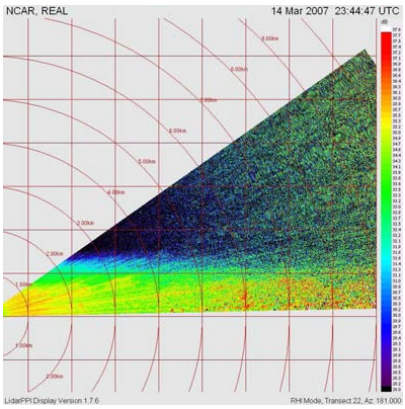

(a) 23:44:47 UTC

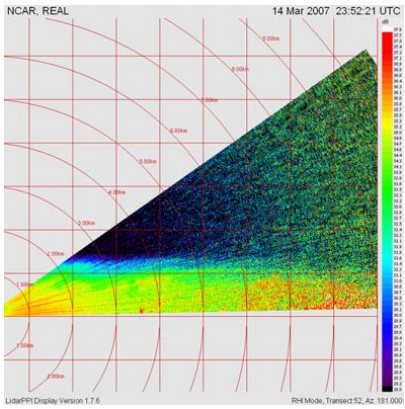

(b) 23:52:21 UTC

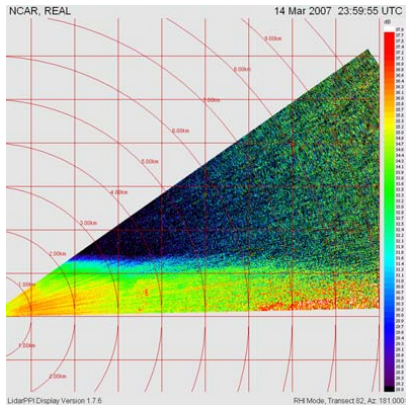

(c) 23:59:55 UTC

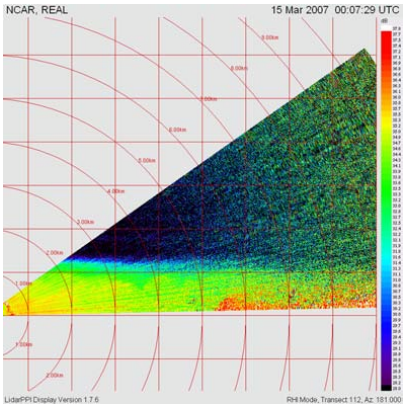

(d) 00:07:29 UTC

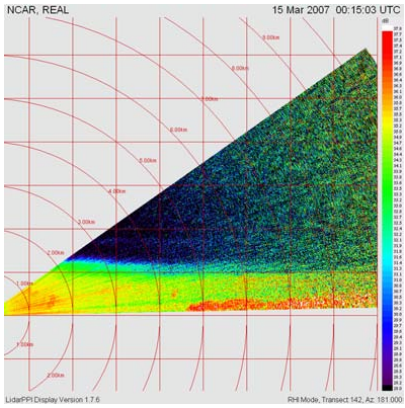

(e) 00:15:03 UTC

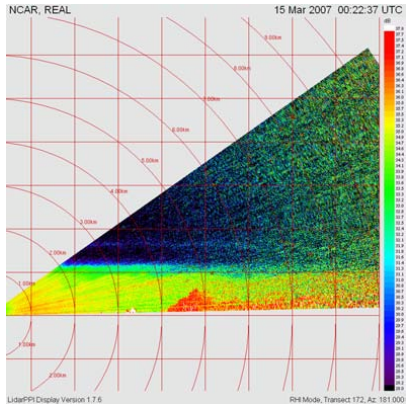

(f) 00:22:37 UTC

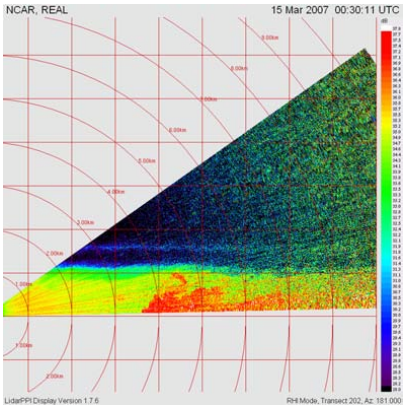

(g) 00:30:11 UTC

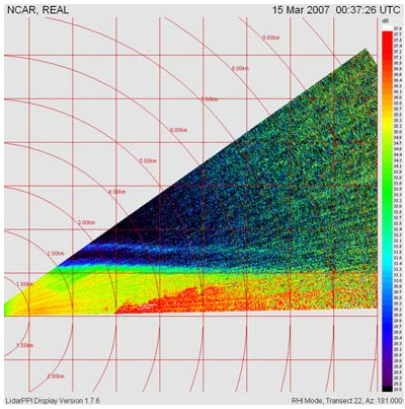

(h) 00:37:26 UTC

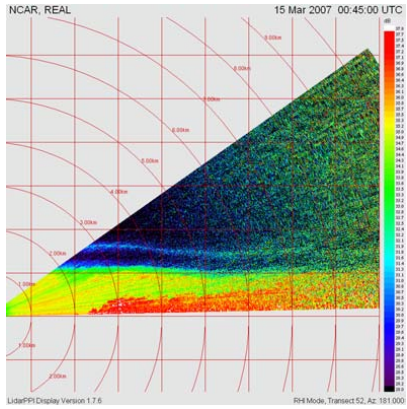

(i) 00:45:00 UTC

Figure 5: Vertical RHI scans from 23:44:47 UTC on 14 March 2007 to 00:45:00 UTC on 15 March 2007. The azimuth angle is 180-degrees (south). Range rings and grid lines are drawn at 1 km intervals. The maximum range shown near the surface is 9 km. See Fig. 6 for a close-up of the front at 01:02:39 UTC.

is from the north. Vertical scans indicate a 1 km deep boundary layer. Figures 4 and 5 show a series of 9 PPI and RHI scans, respectively, during the advancement of this sea-breeze from the south. The sea-breeze comes within observable range of the lidar at approximately 23:44 UTC (at 9 km range), travels to the north, and passes over the lidar site a few minutes after 01:00 UTC on 15 March. Traveling 9 km over 75 minutes indicates a speed of about 2 m s^{-1}. Toward the end of the animation (after 00:40 UTC) we notice that the eastern part of the front advances faster than the western part. Animations of the RHI scans show small billows protruding from the top of the advancing layer—similar in shape to Kelvin-Helmholtz instability billows. An aerosol plume, generated by an unknown source at the surface at approximately 00:21:36 UTC and 3.1 km range is observed to move south and over top of the advancing air-mass. By 00:30:10 UTC, the aerosol plume is located over 800 meters altitude and 4.5 km range. This indicates the southerly component of flow in the immediate vicinity of the front is about 2.7 m s^{-1}.

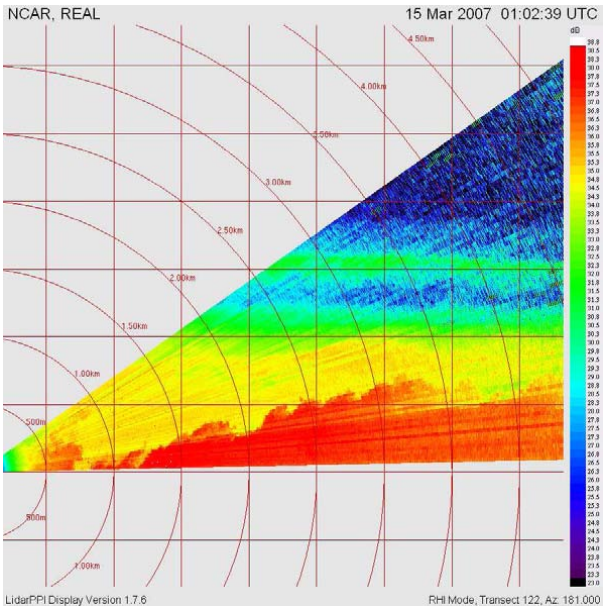

Figure 6: RHI scan from 15 March 2007 at 01:02:39 UTC. Range rings and grid lines are at 500 m intervals. A series of Kelvin-Helmholtz-like billow structures of different scales exist on the top edge of the sea-breeze front. Animations reveal that these structures are very dynamic.

Images 5(g) through 5(i) show a very optically thin aerosol layer at about 1.5 km altitude. This layer undulates as the sea-breeze passes underneath it, revealing how sea-breeze propagation may excite gravity waves in the overlying stable inversion layer. Figure 6 is one RHI scan expanded to show the fine-scale billows on the top edge of the advancing front. In situ observations from the towers located in the orchard were not available at the time of this writing.

4.2 26 April

In this case, the lidar was recording data to a maximum of 5.8 km range. A series of horizontal and vertical cross-sections are shown in Figs. 7 and 8, respectively. The sea-breeze front emerges in the lidar scans at 22:49:18 UTC. The front passes over the lidar site at approximately 23:39:57 UTC. Therefore, it traveled 5.8 km in slightly less than 51 minutes, or an average speed of 1.9 m s^{-1}. RHI scans show that the airmass north of the front is turbulent with aerosol plumes reaching 1.5 km altitude. The RHI scans also show structures resembling Kelvin-Helmholtz billows shearing off the leading edge of the front and moving south. These billows reach altitudes over 1 km at distances of 1.5 to 2.0 km south of the leading edge of the front. Visual inspection of the images reveal that the largest billows have wavelengths on the order of 1 km.

In situ time-series from sensors on the 30 m tall tower indicate that the air temperature dropped abruptly by approximately 2°C and the relative humidity increased by about 12% when this front passed over. The wind direction changed from 320–340° before the arrival of the front to 180–200° after the frontal passage. The wind speed during the hour surrounding the frontal passage did not exceed 5 m s^{-1} at the top of the tower. A closer examination of the in situ data is planned.

4.3 1 May

In this case, the lidar was also collecting data to a maximum of 5.8 km range. A series of horizontal and vertical cross-sections are shown in Figs. 9 and 10, respectively. In contrast to the previous cases, the most remarkable feature of this case is the existence of large wave-like perturbations on the frontal boundary as observed in the *horizontal* scans. The perturbations propagate to the northeast as the frontal boundary advances to the north. The largest of these frontal perturbations have wavelengths of approximately 2 km. Figure 14 shows the progression of the front during a 2-minute period. Large shear billows can also be observed in the RHI scans (Figs. 10(g) through 10(i)). In situ data from the tower in the orchard was available at this time and analysis of it is ongoing.

5. ALGORITHM DEVELOPMENT

Many of the quantities described thus far, such as frontal velocity, air velocity, boundary layer height, and

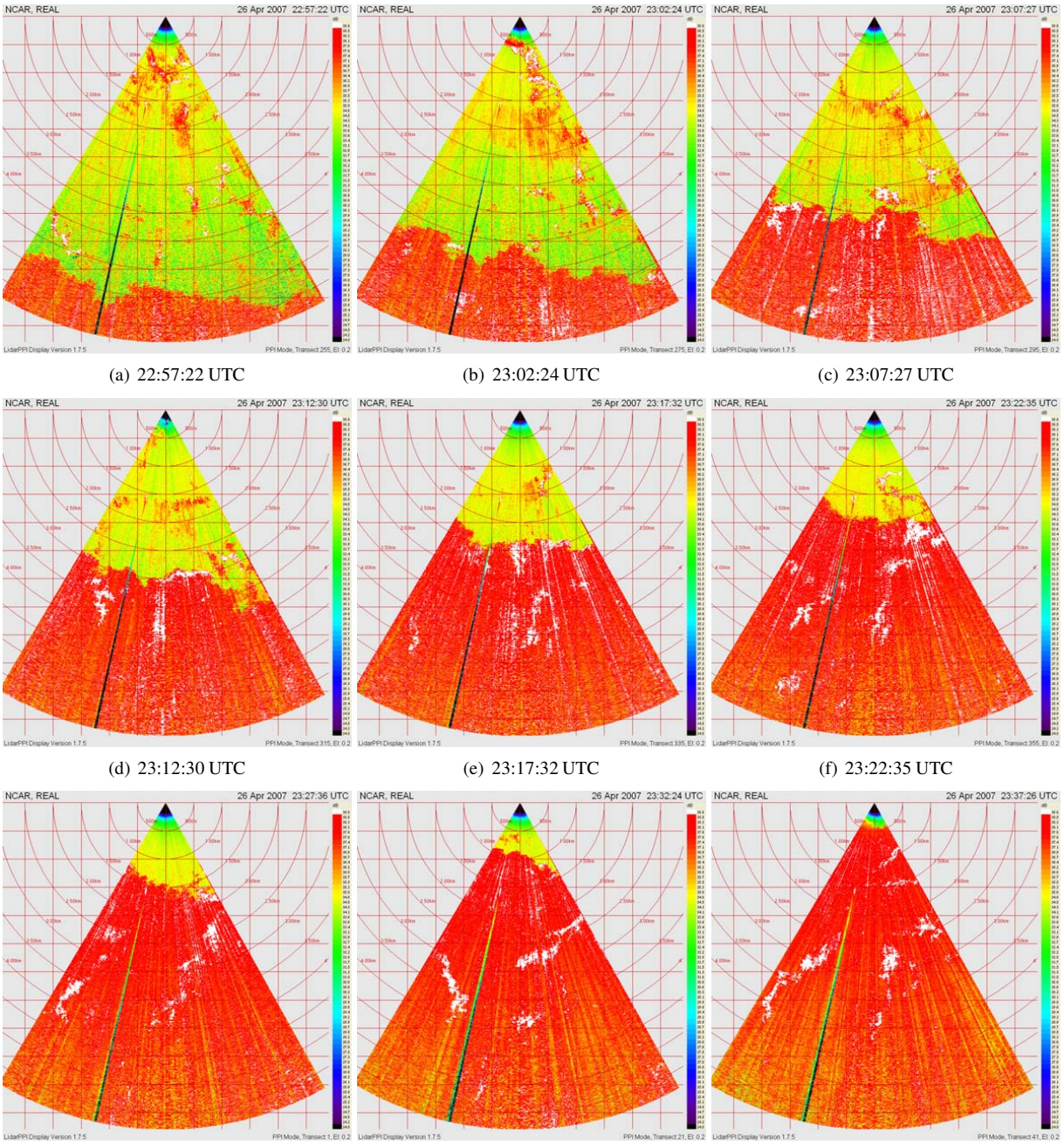

(a) 22:57:22 UTC (b) 23:02:24 UTC (c) 23:07:27 UTC

(d) 23:12:30 UTC (e) 23:17:32 UTC (f) 23:22:35 UTC

(g) 23:27:36 UTC (h) 23:32:24 UTC (i) 23:37:26 UTC

Figure 7: Near-horizontal PPI scans from 22:57:22 UTC to 23:37:26 UTC on 26 April 2007. The elevation angle of the scans is 0.2-degrees above horizontal. Range rings and grid lines are drawn at 500 m intervals. The maximum range shown is 5.8 km.

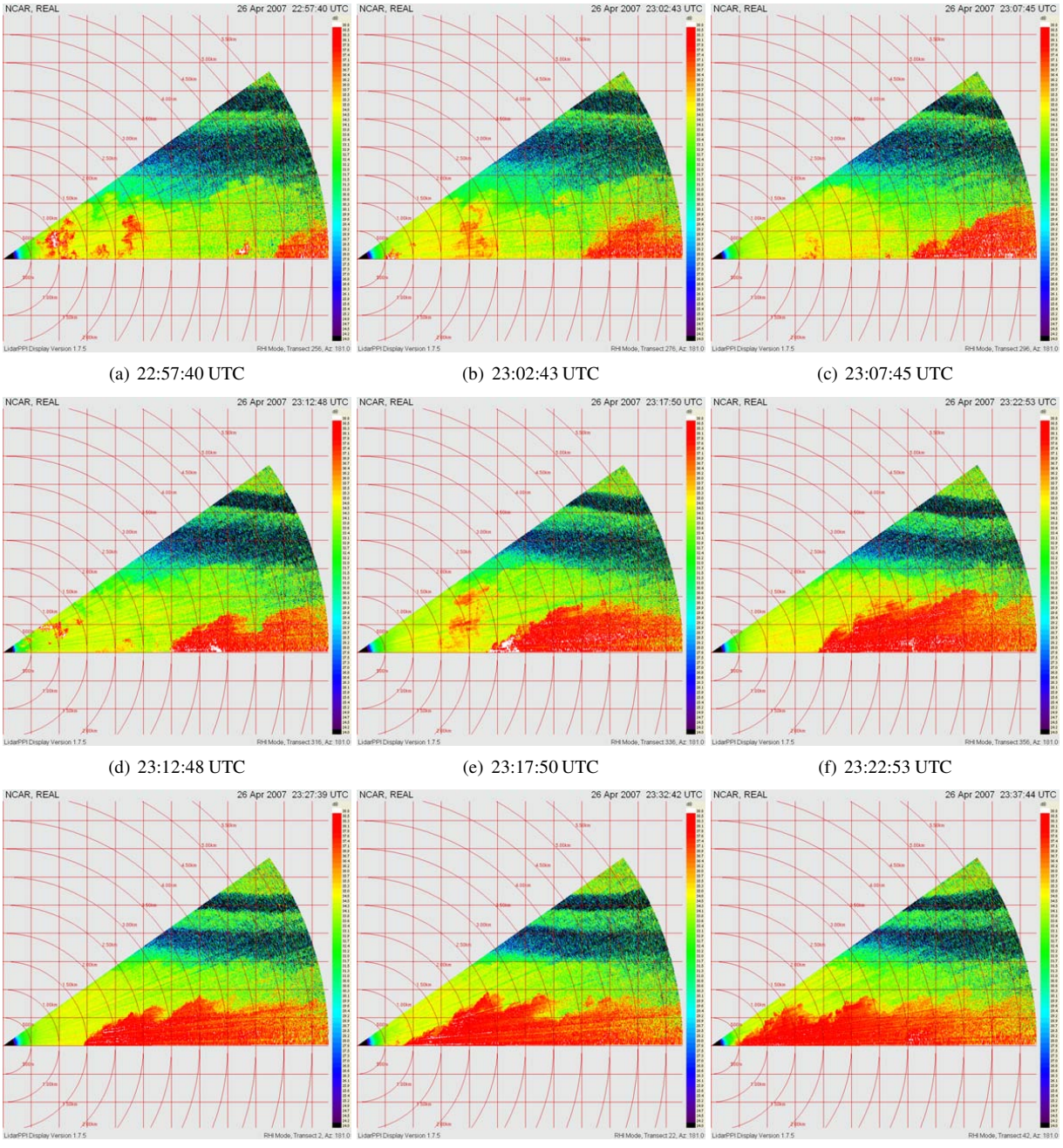

(a) 22:57:40 UTC (b) 23:02:43 UTC (c) 23:07:45 UTC

(d) 23:12:48 UTC (e) 23:17:50 UTC (f) 23:22:53 UTC

(g) 23:27:39 UTC (h) 23:32:42 UTC (i) 23:37:44 UTC

Figure 8: Vertical RHI scans from 22:57:40 UTC to 23:37:44 UTC on 26 April 2007. The azimuth angle is 180-degrees (south). Range rings and grid lines are drawn at 500 m intervals. The maximum range shown is 5.8 km.

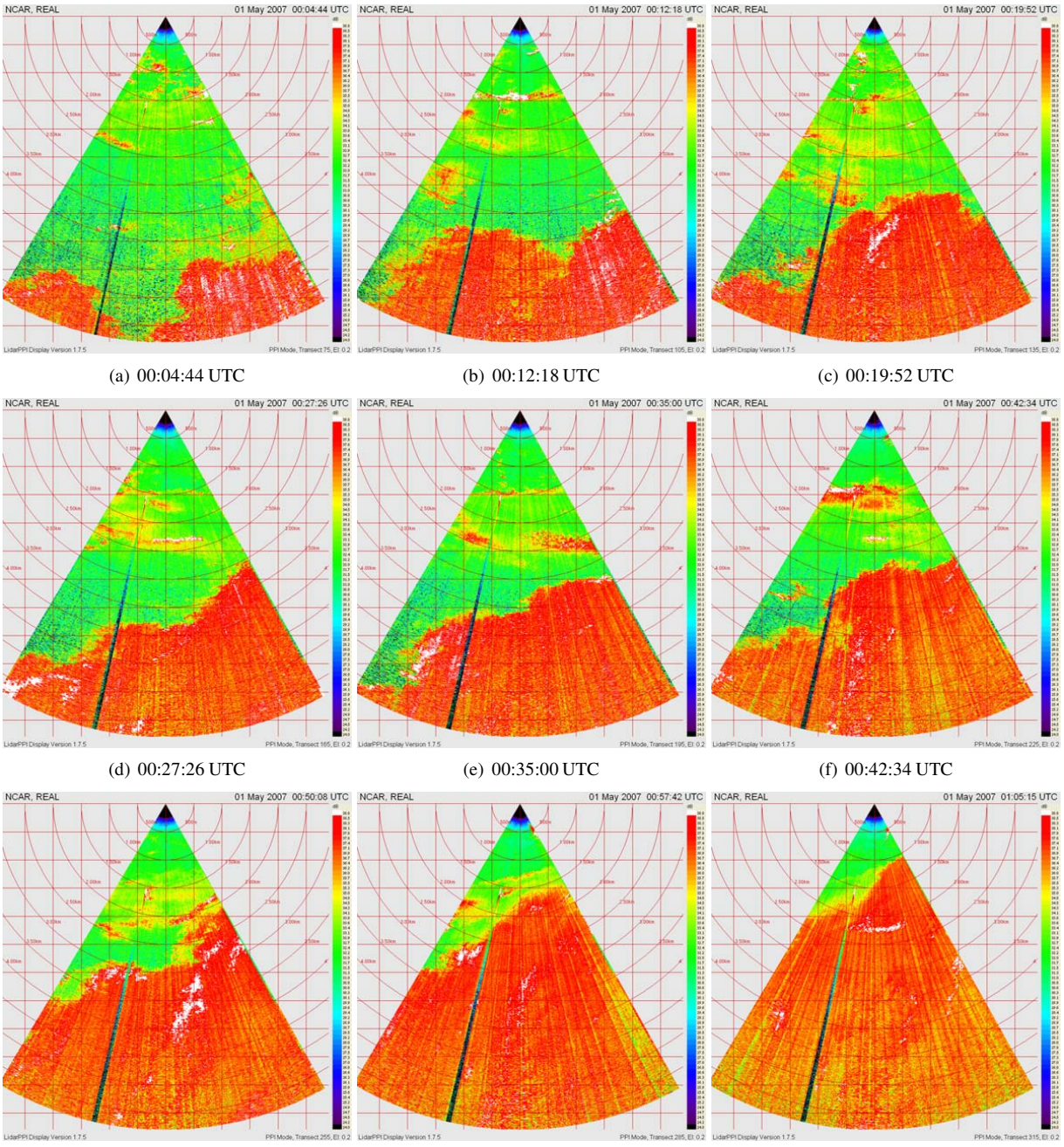

(a) 00:04:44 UTC (b) 00:12:18 UTC (c) 00:19:52 UTC

(d) 00:27:26 UTC (e) 00:35:00 UTC (f) 00:42:34 UTC

(g) 00:50:08 UTC (h) 00:57:42 UTC (i) 01:05:15 UTC

Figure 9: Near-horizontal PPI scans from 00:04:44 UTC to 01:05:15 UTC on 1 May 2007. The elevation angle of the scans is 0.2-degrees above horizontal. Range rings and grid lines are drawn at 500 m intervals. The maximum range shown is 5.8 km.

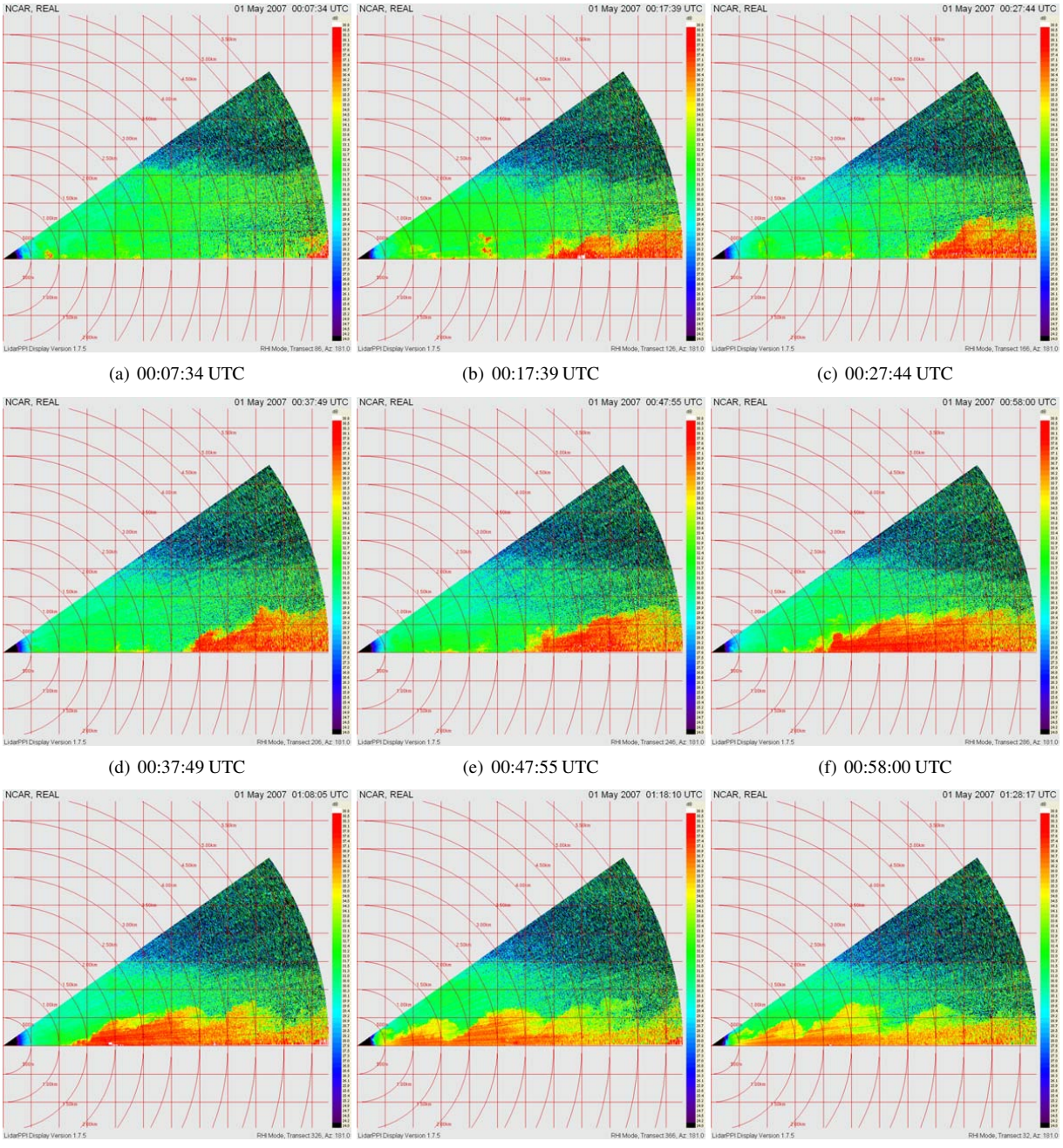

(a) 00:07:34 UTC (b) 00:17:39 UTC (c) 00:27:44 UTC

(d) 00:37:49 UTC (e) 00:47:55 UTC (f) 00:58:00 UTC

(g) 01:08:05 UTC (h) 01:18:10 UTC (i) 01:28:17 UTC

Figure 10: Vertical RHI scans from 00:07:34 UTC to 01:28:17 UTC on 1 May 2007. The azimuth angle is 180-degrees (south). Range rings and grid lines are drawn at 500 m intervals. The maximum range shown is 5.8 km.

wavelength of predominant features, etc., were determined by subjective visual inspection of the lidar images. In the future, we expect to be able to derive these quantities objectively via the application of algorithms. For example, if the position of the front can be objectively determined by an algorithm, then its velocity and change of shape can be more precisely determined. Similarly, if variations in the aerosol backscatter can be correlated between displaced frames, then a field of motion vectors may be produced to describe the flow. This can be performed on both sides of the front. When used together, a more complete picture of the kinematics of air motion around these types of fine-scale boundaries should be possible. In the next two sections, we describe recent progress on this subject.

5.1 Wavelets

We applied the Haar wavelet algorithm, described in detail by Davis et al. (2000), to identify the leading edge of the sea-breeze. For the three cases presented in this paper, the airmass beyond the leading edge of the gust front is evidenced with high aerosol backscattering. The front itself creates a step-like feature in the backscatter data — very similar in gradient to the top edge of an aerosol rich boundary layer in vertically pointing lidar data. Therefore, a Haar wavelet with large (1 km) dilation can be applied to each radial beam of backscatter data. Use of a large dilation provides a robust identification of the front—provided that the beam does indeed intersect the front. Smaller dilations result in the identification of small aerosol plumes associated with surface sources. Figure 11 shows the location of the front as determined by the wavelet algorithm for one scan on 1 May 2007. Note that the algorithm robustly identifies the edge of the front and not the aerosol plumes at closer ranges. Figures 12 and 13 show the advancement of the fronts from successive scans on 15 March and 26 April, respectively. The horizontally propagating waves on the frontal boundary on 1 May make a similar diagram difficult to interpret. As a result, we have plotted just 5 successive scans over a 2 minute period to show the wave-like motion of the front in Fig. 14. These perturbations are likely to have a strong effect on the lateral entrainment rate.

By applying the wavelet technique to these scans, we can track the position of the sea-breeze front. Doing so allows us to extract the velocity of the boundary itself, and perturbations on the boundary.

5.2 Wind Vectors

We are currently developing software to apply the correlation method to derive horizontal vector motion of the aerosol variability. This technique was described by

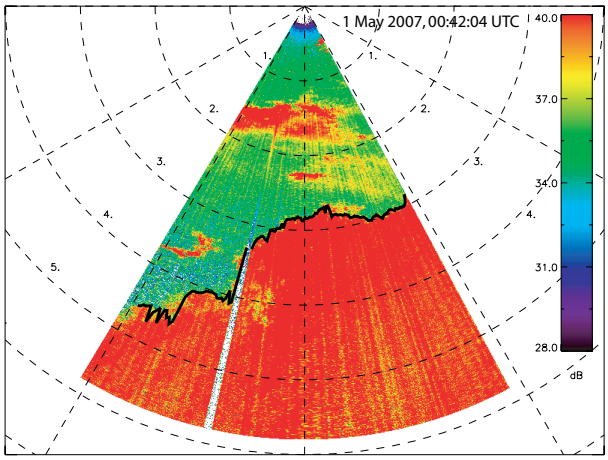

Figure 11: Location of the sea-breeze front (thick black line) on the PPI scan ending at 00:42:04 UTC on 1 May 2007 as determined by the wavelet algorithm.

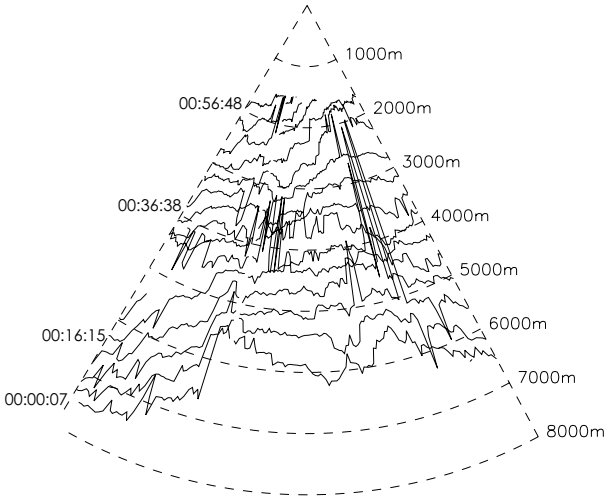

Figure 12: Location of the sea-breeze front on 15 March 2007 as determined by the wavelet algorithm for successive scans.

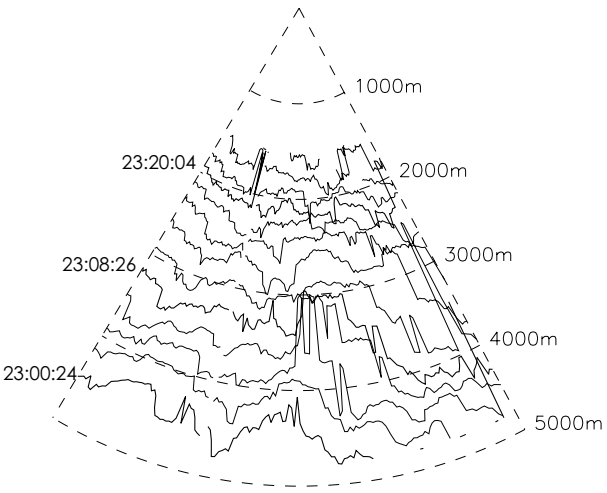

Figure 13: Location of the sea-breeze front on 26 April 2007 as determined by the wavelet algorithm for successive scans.

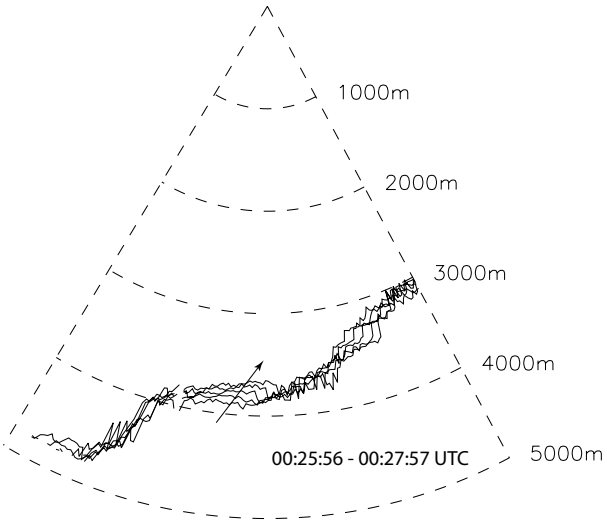

Figure 14: Location of the sea-breeze front on 1 May 2007 as determined by the wavelet algorithm for 5 successive scans. The arrow was subjectively drawn to indicate movement of the frontal position.

Sasano et al. (1982) and Mayor and Eloranta (2001). Although similar in approach to Mayor and Eloranta (2001), the software used to derive flow vectors for the REAL data is entirely new, incomplete and untested at the time of this writing. The key advancement over Mayor and Eloranta (2001) is that the software has been entirely re-written in the QT4 programming language. It now has the ability to operate in real-time and produce vector fields that are updated on every scan. Currently, the software is functional but incomplete. The steps of temporal median filtering, histogram normalization, and fitting a surface to the correlation function will be implemented next. We intend to check the resulting vectors with in situ measurements of wind from the tower.

6. CONCLUSIONS

Although elastic backscatter lidar observations of sea-breeze fronts are not new, they are rare. Nakane and Sasano (1986) published what appear to be the first observations of sea-breeze fronts. Other works include Kolev et al. (1998). It is likely that simultaneously achieving eye-safety and sufficient performance has been a limitation thereby preventing more of these types of observations. Recent breakthroughs in lidar technology at 1.5-microns wavelength during the last 5 years enabled us to collect a remarkable 3-month meteorological data set in 2007 in support of CHATS. The key technology breakthroughs in REAL include excellent elastic backscatter lidar performance with scanning, eye-safety at all ranges, and continuous and unattended operation. Although the backscatter intensity measurements are uncalibrated, the images contain extremely useful spatial and temporal information that would have been difficult or impossible to obtain with other instruments. The information includes vertical and horizontal structure, feature location, movement, and deformation. Time-lapse animations of the images are an important data analysis product, but cannot be shown in a paper.

We intend to continue our analysis of this data set, especially for turbulent coherent structures just above the canopy. We will relate the lidar backscatter data to the in situ observations. The data set should be of particular value to studies such as those by Plant and Keith (2007). We will also continue to improve the performance of REAL and develop software to make analysis of the data easier and more useful to a broader array of users and applications.

REAL is available for use by the university community. For more information on how to request REAL, please contact the NSF Division of Atmospheric Sciences. For more information on the instrument, please go to: www.lidar.ucar.edu.

Acknowledgements

The deployment of REAL to CHATS was funded by the 2007 NCAR Director's Opportunity Fund. NCAR is sponsored by the National Science Foundation. The authors thank Mr. Bob Currey and the Gnos family for allowing us to operate REAL on their land. Anna Petrova-Mayor assisted with the typesetting of this paper.

REFERENCES

Davis, K. J., N. Gamage, C. R. Hagelberg, C. Kiemle, D. H. Lenschow, and P. P. Sullivan, 2000: An objective method for deriving atmospheric structure from airborne lidar observations, *J. Atmos. Ocean. Technol.*, **17**, 1455–1468.

de Boer, G., 2004: *Nested high resolution simulation and lidar validation of a land breeze circulation*, Master's thesis, University of Wisconsin, Madison.

de Boer, G., E. W. Eloranta, and G. J. Tripoli, 2004: Nested high resolution simulation and lidar validation of a land breeze circulation, in *16th Symp. on Boundary Layers and Turbulence*, AMS.

—, 2005: Lidar validation of numerical simulations of a Lake Michigan land breeze, in *2nd Symposium on Lidar Atmospheric Applications*, AMS.

Kolev, I., O. Parvanov, B. Kaprielov, E. Donev, and D. Ivanov, 1998: Lidar observations of sea-breeze and land-breeze aerosol structure on the Black Sea, *J. Appl. Meteor.*, **37**, 982–995.

Mayor, S. D. and E. W. Eloranta, 2001: Two-dimensional vector wind fields from volume imaging lidar data, *J. Appl. Meteor.*, **40**, 1331–1346.

Mayor, S. D. and S. M. Spuler, 2004: Raman-shifted eye-safe aerosol lidar (REAL), *Appl. Optics*, **43**, 3915–3924.

Mayor, S. D., S. M. Spuler, B. M. Morley, and E. Loew, 2007: Polarization lidar at 1.54-microns and observations of plumes from aerosol generators, *Opt. Eng.*, **46**, In press.

Nakane, H. and Y. Sasano, 1986: Structure of a sea-breeze front revealed by scanning lidar observation, *J. Meteor. Soc. Japan*, **64**, 787–792.

Plant, R. S. and G. J. Keith, 2007: Occurrence of Kelvin-Helmboltz billows in sea-breeze circulations, *Bound. Layer Meteor.*, **122**, 1–15.

Sasano, Y., H. Hirohara, T. Yamasaki, H. Shimizu, N. Takeuchi, and T. Kawamura, 1982: Horizontal wind vector determination from the displacement of aerosol distribution patterns observed by a scanning lidar, *J. Appl. Meteor.*, **21**, 1516–1523.

Spuler, S. M. and S. D. Mayor, 2005: Scanning eye-safe elastic backscatter lidar at 1.54 microns, *J. Atmos. Ocean. Technol.*, **22**, 696–703.